Quantum-inspired space-time PDE solver and dynamic mode decomposition

Raghavendra D. Peddinti,¹ Stefano Pisoni,^{1,2} Narsimha Rapaka,³ Mohamed K. Riahi,³ Egor Tiunov,¹ and Leandro Aolita¹

¹ Quantum Research Center, Technology Innovation Institute, Abu Dhabi, UAE

² Institute for Quantum-Inspired and Quantum Optimization,

Hamburg University of Technology, Germany

³ Emirates Nuclear Technology Center (ENTC),

Khalifa University of Science and Technology, Abu Dhabi, UAE

(Dated: October 28, 2025)

Numerical solutions of partial differential equations (PDEs) are central to the understanding of dynamical systems. Standard approaches involving time-stepping schemes compute the solution at each time step, which becomes too costly when simulating long-term dynamics. Alternatively, spacetime methods that treat the combined space-time domain simultaneously promise better stability and accuracy. Interestingly, data-driven approaches for learning and predicting dynamics, such as dynamic mode decomposition (DMD), also employ a combined space-time representation. However, the curse of dimensionality often limits the practical benefits of space-time methods. In this work, we investigate quantum-inspired methods for space-time approaches, both for solving PDEs and for making DMD predictions. We achieve this goal by treating both spatial and temporal dimensions within a single matrix product state (MPS) encoding. First, we benchmark our MPS space-time solver for both linear and nonlinear PDEs, observing that the MPS ansatz accurately captures the underlying spatio-temporal correlations while having significantly fewer degrees of freedom. Second, we develop an MPS-DMD algorithm to make accurate long-term predictions of nonlinear systems, with runtime scaling logarithmically in both spatial and temporal resolution. This research highlights the role of tensor networks in developing effective and interpretable models, bridging the gap between numerical methods and data-driven approaches.

I. INTRODUCTION

Numerical solutions of partial differential equations (PDEs) are of great importance in studying dynamical systems. However, obtaining highresolution numerical solutions is often prohibitively expensive due to the curse of dimensionality [1] This problem motivated the application of tensor networks in the development of efficient numerical methods [2–4]. In previous works [5–12], the key idea consists of compressing the spatial information of the solution using a 1D tensor network known as matrix product states (MPSs) or tensor trains (TTs) [13– 15]. The time evolution is then performed within the compressed representation, using efficient linear algebra subroutines [16–18]. The efficiency of these methods stems from the ability of MPSs to exploit the nature of spatial correlations [19–21]. Despite their promising compression rates, these approaches rely on expensive time-stepping schemes that limit the total simulation duration. The restriction on the size of the time step τ arises from stability criteria, such as the Courant-Friedrichs-Lewy condition [22].

Naturally, this has prompted the exploration of alternatives such as space-time methods. Space-time methods differ from time-stepping methods by treating time as an additional spatial dimension [23, 24]. The simultaneous treatment of the space-time domain offers better stability and improved accuracy at

the cost of increased memory and runtime [25]. Tensor networks provide a powerful tool for efficiently handling the entire space-time solution. In fact, recent works have explored the development of tensor network-based space-time solvers [26–30]. However, the characterization of spatio-temporal correlations remains incomplete. As a result, the efficiency of tensor networks in the context of space-time solvers is still an open question.

Interestingly, data-driven approaches to learning and predicting dynamics, such as the dynamic mode decomposition (DMD), also benefit from a combined space-time representation of the data [31, 32]. DMD is a powerful tool that extracts the dynamically relevant spatial modes from the time series of the system's historical states. These modes can then be used to predict the future dynamics efficiently. However, the DMD algorithm scales linearly with both spatial and temporal resolution of the time series. This opens up an interesting avenue for representing the data with tensor networks, enabling efficient and accurate predictions.

In this work, we investigate MPS-based spacetime methods from both perspectives: simulation and data-driven prediction of dynamical systems. First, we introduce an MPS-based space-time method for solving both linear and nonlinear PDEs. We benchmark our MPS space-time solver for a variety of (1+1)D PDEs arising from both classical and quantum physics. Here, we study the spatial and temporal correlations by computing the entanglement entropy of the MPS. For all tested equations, we observe that the MPS representation captures the relevant spatio-temporal characteristics using parameters less than 1% of the grid size. Second, for data-driven prediction, we observe that the MPS space-time encoding offers a natural ground for computing the dynamic mode decomposition (DMD). This allows us to develop an MPS-DMD algorithm whose complexity scales logarithmically with both spatial and temporal resolution. We accurately predict the long-term dynamics of nonlinear systems such as the Burgers' equation and the Karman vortex street. The benefits of this connection are twofold: first, MPS-DMD facilitates quick and accurate predictions necessary for real-world applications. Second, this reveals the inherent structure of the MPS encoding, thereby enhancing its interpretability as a compressed representation. Under the assumption of low temporal entanglement, our findings would enable exponential runtime speedups over the standard PDE solvers and DMD methods.

II. PRELIMINARIES

A. Connection with previous works

We briefly summarize the recent developments of tensor network-based space-time solvers. Dolgov et al. [26] implemented one of the first global space-time formulations in the TT format. Breiten et al. [27] implemented a TT space-time method for solving a nonlinear control problem. Following this, Adak et al. [28, 29] demonstrated the advantages of TT space-time solvers for both linear and nonlinear transport problems. Recently, Arenstein et al. [30] studied the 1D Burgers' equation, showing clear advantages over standard time-stepping schemes. In this work, we study several PDEs, including the Burgers' equation, and independently observe similar advantages. In contrast, none of the earlier works tackle DMD directly from the MPS spacetime encoding. Although Klus et al. [33] developed a tensor-based DMD algorithm, it differs critically in its treatment of the time dimension.

B. Space-time methods

We introduce the standard space-time formulation for solving a (1+1)-dimensional time-dependent PDE of u defined on the domain $(x,t) \in \Omega \times (0,T]$,

given by:

$$\partial_t^p u + F(u, \partial_x u, \dots, \partial_x^q u) = g(x, t) \tag{1}$$

where F is a function of u and its partial derivatives up to order q. ∂_t^p refers to the p-th derivative in time (usually, p=1 or 2), and g(x,t) defines the source term. The corresponding initial and boundary conditions are given by $u_0(x)$ (and $\partial_t u(x,t)|_{t=0}$ for the second derivative in time) and $u(x,t)|_{\partial\Omega}$, respectively. After discretization, the objective is to find the solution simultaneously for all $N_x \times N_t$ points in the discretized domain $\{h,...,N_xh\} \times \{\tau,...,N_t\tau\}$, where $h = |\Omega|/N_x$ and $\tau = T/N_t$.

First, we use a finite difference scheme to compute the time derivative with forward differences and the spatial derivatives with central differences. Next, we build the *all-at-once* system by assembling the discretized space and time operators of Eq. (1) using the tensor product (\otimes) . The resulting system, along with the appropriate initial and boundary condition terms $\mathcal{I}(u)$, $\mathcal{B}(u)$, is given by:

$$(\mathbb{I}_x \otimes \mathbb{D}_t^p + \mathbb{F}_x(u) \otimes \mathbb{I}_t) \mathbf{u} = \mathbf{g} + \mathcal{I}(u) + \mathcal{B}(u), \quad (2)$$

where \mathbb{I} is the identity operator, \mathbb{D}_t^p is the discretized time derivative of order p, and $\mathbb{F}_x(u)$ is the discretized spatial operator as a function of u. Here, u and g denote the discretized versions of u(x,t) and g(x,t), which are vectorized as:

$$\mathbf{u} = (u_{1,1}, u_{1,2}, ..., u_{1,N_t}, u_{2,1}, ..., u_{N_x,N_t})^T$$
 (3)

where, $u_{i,j} = u(ih, j\tau)$ and analogously for g. Moreover, Eq. (2) can be solved with a linear system solver only if the equation is linear, i.e., \mathbb{F}_x is independent of u. For nonlinear PDEs, the algebraic system is linearized according to the Picard iterative scheme [34]. This is implemented by replacing the dependence of $\mathbb{F}_x(u)$ by the solution at previous iteration, i.e., $\mathbb{F}_x(u^{(p-1)})$ at iteration p. The initial guess is chosen by repeating the initial condition for all time steps: $u^{(0)} = u_0 \otimes I_t$.

Throughout our work, we employ the implicit formulation of the problem. In Appendix A, we present the detailed construction of the all-at-once linear system for both linear and nonlinear equations. Additionally, we note that the generalization to higher dimensions follows a similar construction.

C. Dynamic mode decomposition:

Dynamic mode decomposition (DMD) is a datadriven technique used to analyze nonlinear systems, revealing their underlying spatiotemporal characteristics through spectral analysis. Initially developed within the fluid dynamics community [31], the DMD toolbox has since expanded and found applications in various fields, including robotics, quantum physics, neuroscience, and data processing [35–37]. The success of DMD is theoretically underpinned by its connection with Koopman operators and their spectra. For more details, we recommend the reader refer to these outstanding reviews [32, 38].

In Algorithm 1, we summarize the standard DMD algorithm. This assumes two discrete time series of states $u_j \doteq u(\cdot, j\tau) \in \mathbb{R}^{N_x}$, one starting at time j = 0 and the other one at time j = 1, arranged respectively into X and X' in $\mathbb{R}^{N_x \times N_t}$, known as snapshot matrices. The (possibly nonlinear) dynamics between X and X' are approximated by a linear evolution operator A. First, the singular value decomposition, also known as proper orthogonal decomposition (POD), of X is computed. The singular values Σ are then used to compute the pseudoinverse X^+ , and $A := X'X^+$ is given by $X'V^{\dagger}\Sigma^{-1}U$. By projecting A onto the span of the left singular values U, one obtains a $|\Sigma| \times |\Sigma|$ matrix A. By computing the eigen decomposition of \tilde{A} , the dynamic modes Φ of the data are found. These modes are then used to predict the future evolution of the system without having to solve any PDE. Moreover, in practice, Σ is usually truncated to keep the r most significant singular values, resulting in r dynamic modes. This leads to an efficient approximation of A that is often very accurate, even for $r \ll |\Sigma|$.

Algorithm 1: DMD

Require: Snapshot matrices

 $X = [\boldsymbol{u}_0, \dots, \boldsymbol{u}_{N_t-1}], X' = [\boldsymbol{u}_1, \dots, \boldsymbol{u}_{N_t}];$ $X, X' \in \mathbb{R}^{N_x \times N_t}$

Ensure: $X' = AX \implies A := X'X^+$ where X^+ is the pseudoinverse of X.

- 1: Proper orthogonal decomposition: $X = U\Sigma V^{\dagger}$, with rank $|\Sigma|$
- 2: Project A onto the span of U: $\tilde{A} = U^{\dagger}AU = U^{\dagger}X'V\Sigma^{-1} \in \mathbb{R}^{|\Sigma| \times |\Sigma|}$
- 3: Eigen decomposition: $\tilde{A}W = W\Lambda$
- 4: Compute the dynamic modes:
 - $\Phi = UW \in \mathbb{C}^{N_x \times |\Sigma|}$

return (Λ, Φ)

III. RESULTS

As shown in Fig. 1, we develop two methods to simulate and predict dynamics: MPS space-time solver and MPS-DMD, respectively. We first introduce the MPS space-time encoding. We then present the details of our MPS space-time solver, along with the numerical simulations of both linear and non-linear PDEs. Finally, we introduce the MPS-DMD

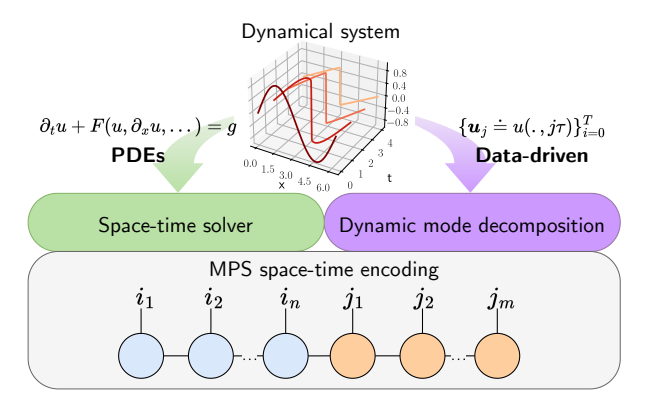


FIG. 1. Overview of simulation and prediction of dynamical systems, using the MPS space-time encoding. Let u(x,t) denote the state of the dynamical system. The evolution of the state can be simulated by solving the governing equations, given by time-dependent PDEs. Alternatively, the dynamics can be predicted by learning from the system's historical data, as represented by the time series. Using the matrix product state (MPS) encoding over the combined space-time domain, we develop the MPS counterparts of the space-time solver and dynamic mode decomposition.

algorithm and predict long-term dynamics of non-linear systems such as the Karman vortex street.

A. MPS space-time encoding

We briefly introduce the MPS space-time encoding. Let M denote a 2D array of size $N_x \times N_t$, representing either a discretized function or time series data. It is assumed, without loss of generality, that x and t dimensions are powers of two, i.e., $N_x = 2^n$; $N_t = 2^m$. Next, we split i, j indices into their respective binary indices $\{i_1, ..., i_n\}$ and $\{j_1, ..., j_m\}$. Then, M is decomposed into an MPS representation such that each element $M_{i,j}$ is given by a product of matrices:

$$M_{i,j} = A_1^{(i_1)} A_2^{(i_2)} \dots A_n^{(i_n)} A_{n+1}^{(j_1)} A_{n+2}^{(j_2)} \dots A_{n+m}^{(j_m)},$$
(4)

where $A_l^{(0)}$ and $A_l^{(1)}$ constitute the 2(n+m) matrices of sizes $\chi_{l-1} \times \chi_l$, with χ_0 and χ_{n+m} equals to 1. Also, i_l and j_l are referred to as the *physical indices*, and the matrix indices of A_l are known as the *virtual indices* of the MPS. The bond dimension (χ) is defined as the maximal dimension over all virtual indices. We note that the order of the binary indices is a matter of convention, and other permutations of indices are also possible. Unless otherwise specified, we follow the *space-time ordering*, shown in Eq. (4) and presented graphically in Fig. 1. This choice corresponds to Eq. (3) in a vectorized form.

χ	Parameters	Residual	Iterations
Heat equation			
$u_t - \alpha u_{xx} =$: 0		
2	0.009%	4.1×10^{-3}	(1, 4)
Wave equation			
$u_{tt} - ku_{xx} =$	= 0		
2	0.014%	1×10^{-2}	(1, 4)
Burgers' equation			
$u_t + uu_x - \nu u_{xx} = 0$			
10	0.25%	1.2×10^{-3}	(4, 4)
Nonlinear Diffusion equation			
$u_t - (\kappa(u)u_x)_x = 0$			
10	0.25%	4.9×10^{-6}	(4, 4)
Nonlinear Schrödinger equation			
$i\psi_t + \psi_{xx} + 2 \psi ^2\psi = 0$			
10	0.27%	2.6×10^{-4}	(12, 4)

TABLE I. Summary of numerical simulations for both linear and nonlinear PDEs. We present the performance of the MPS space-time solver, using a 20-qubit MPS for a 1024×1024 grid in x-t. In the first column, we present the bond dimension of the MPS solution. Next, we report the total number of parameters in the MPS as a percentage of the grid size. Finally, we present the residual $(\|Ax-b\|_2/\|b\|_2)$ of the solution at the final iteration, where the total number of iterations is the product of the *outer* Picard updates (p) and the *inner* DMRG sweeps (s), presented as (p,s). In App. B, we present the initial and boundary conditions, as well as a comparison with analytical solutions.

B. MPS space-time solver

First, we introduce the MPS space-time solver, following the outline presented in Sec IIB. Starting with the discretization of the domain, we represent the discretized functions in Eq. (2) with the corresponding space-time MPSs and the finite difference operators with matrix product operators (MPOs). Similarly, the boundary and initial conditions are also encoded into the MPS space-time representation. All of the necessary MPSs and MPOs are either constructed analytically [17, 39] or found numerically using TT-SVD [15] or TT-cross interpolation [40, 41]. Finally, we assemble the all-at-once linear system and solve it using DMRG-inspired methods [16, 42]. We present a detailed construction of the linear system in App. A. In Table I, we summarize the performance of the MPS space-time solver for both linear and nonlinear PDEs. In App. B, we discuss the initial and boundary conditions along with comparisons with analytical solutions.

Next, we discuss the effectiveness of the MPS space-time solver, providing numerical evidence to support our arguments. The efficiency of the MPS

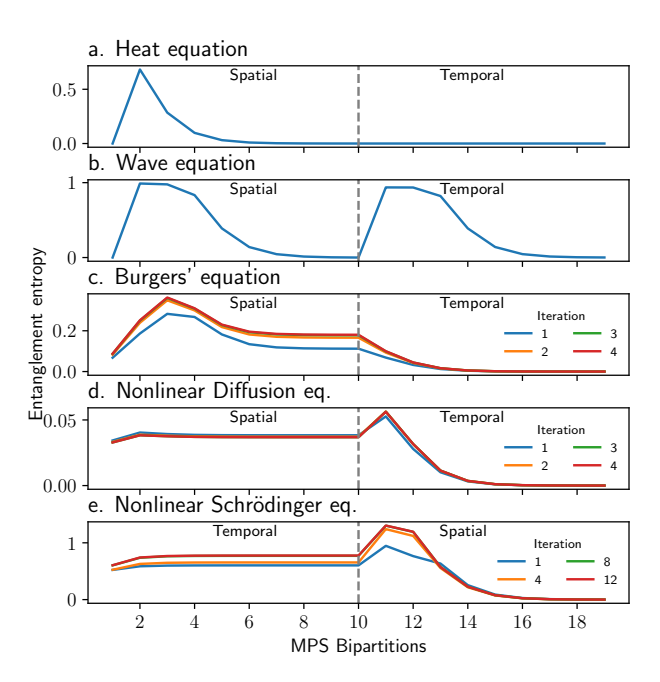


FIG. 2. Entanglement entropy of the MPS space-time solution. We present the bipartite entanglement entropy as a measure of spatio-temporal correlations captured by the MPS ansatz. For linear equations, we plot the entanglement of the final solution. For nonlinear equations, we plot the intermediate iterations of the Picard scheme. For all PDEs, we use a 20-qubit MPS encoding to represent the solution on a 1024×1024 spacetime grid. The numerical simulations are summarized in Table I, and initial and boundary conditions are presented in Appendix B. We exceptionally use the time-space ordering for the nonlinear Schrödinger equation, which is further explained in Appendix C.

space-time solver depends on two factors: (a) the bond dimension of the MPS space-time solution and (b) the convergence of the DMRG solver and the Picard iterative scheme.

a. Bond dimension and compressibility: To estimate the compressibility, we compute the bipartite entanglement entropy $S_{A|B}$ of the MPS space-time solution given by $S_{A|B} = -\sum_{j=1}^{\chi} s_j^2 \log_2 s_j^2$, where s_j are the Schmidt coefficients at the bond partitioning the MPS into subsets A and B (See Ref. [2]) for more details). We note that the entanglement entropy S is upper bounded by $\log(\chi)$. For each bipartition of the MPS, the corresponding entanglement entropy is interpreted differently. For bonds connecting the spatial tensors, S determines the interscale correlations in space. Similarly, for temporal tensors, the bonds capture the interaction between slow and fast dynamics of the system. For the bond connecting the spatial and temporal tensors, S captures the separability of variables x and t. This is particularly insightful because the notion of separability is fundamental to the study of PDEs. For instance, in linear PDEs, such as the heat equation, the separation of variables yields a set of independent ODEs for each variable. Even for nonlinear PDEs, separability remains powerful in finding analytical solutions, with special conditions [43].

In Fig. 2, we present the entanglement entropy of the MPS space-time solution for the PDEs summarized in Table I. In Appendix B, we present the specific initial and boundary conditions, along with a detailed comparison with analytical solutions, wherever available. Here, we restrict our discussion to the chosen instances of the PDEs. For the heat equation in panel a, we observe that the exponential decay of the solution in time results in a separable temporal part, and the independence of the x and t variables is also evident. In panel b, we observe that the spatial correlations exhibit a similar trend to the temporal part. This captures the equivalence of x and t variables present in the wave equation and its solution. We also see that the space-time parts are weakly entangled with each other, as the solution remains separable along the characteristic coordinates of $x \pm ct$.

For nonlinear equations, in panels c-e, we notice an immediate jump in entanglement between the spatial and temporal parts of the MPS. Despite this, the bond dimension remains small, with the total number of MPS parameters being less than 1% of the grid size. For both Burgers' and nonlinear diffusion equations, we observe that the temporal entanglement decays quickly, indicating a smooth evolution trajectory. For the 1D nonlinear Schrödinger equation in its focusing regime, we note that the temporal entanglement in this case does not decay but remains almost constant, which is a result of the time-space ordering of the MPS. This choice is motivated by the observed improvement in the stability of the iterative solver, as explained in Appendix C.

b. Convergence and runtime: We note that the MPS representation is not only efficient in memory but also enables efficient linear algebraic operations that scale logarithmically with the grid size and polynomially with the bond dimension [15]. The all-at-once linear systems are also solved efficiently due to the logarithmic scaling of the runtime of DMRG-inspired solvers [16, 42]. The convergence of the Picard iteration is guaranteed by the Picard-Lindelöf theorem and is linear in the number of iterations [34, 44]. By substituting the Picard linearization with the Newton method, we can improve the convergence quadratically. Additionally, in Ref. [45], we conduct an exhaustive benchmarking of an MPS space-time solver based on the Newton method, for nonlinear PDEs in several regimes.

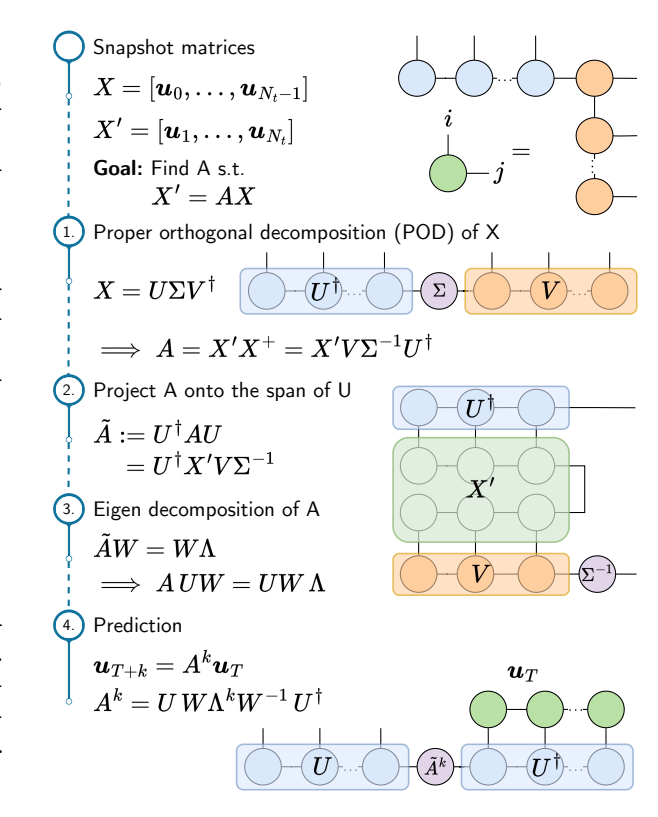


FIG. 3. MPS-DMD algorithm. We assume that the snapshot matrices X and X' are provided in their MPS representations. First, we compute the proper orthogonal decomposition (POD) of X by bringing the corresponding MPS into the mixed canonical form at the bond connecting the spatial and temporal parts. Now, the pseudoinverse of X, denoted by X^+ , can be computed by inverting the singular values Σ . We then project A onto the span of U to obtain the reduced evolution operator A, which is used to efficiently compute the eigen decomposition of the full operator A. We further use this decomposition to predict the future evolution of the system. All of the matrix operations, except for the eigen decomposition of \tilde{A} , are computed with only local contractions, resulting in a logarithmic scaling with both the spatial resolution and the number of snapshots.

C. MPS-DMD

Here, we develop an MPS-based method to compute the dynamic mode decomposition. We start with the assumption that the snapshot matrices are provided in their corresponding MPS space-time encoding. Later, we discuss efficient methods to convert arbitrary data into the required MPS format. Next, we see that the gauge freedom of the MPS representation can be exploited to compute the POD of $X := U\Sigma V^{\dagger}$. We achieve this by changing the gauge of its MPS into the mixed canonical form [2], centered at the space-time bond. We note that this is

equivalent to the Schmidt decomposition from the Quantum Physics literature. As shown in Fig. 3, the isometries U and V^{\dagger} of sizes $N_x \times r$ and $r \times N_t$, respectively, are given by the corresponding MPS tensors after the gauge transformation. And, Σ is a diagonal matrix provided by the singular values at the space-time bond of the MPS, which corresponds to choosing $r = \chi$ from Alg. 1. As discussed in Sec. III B, since the spatio-temporal entanglement is typically low, one expects $\chi \ll N_x$.

We then compute the (approximate) evolution operator $A = X'X^+ \in \mathbb{R}^{N_x \times N_x}$. Here, X^+ is the pseudoinverse of X, which is obtained directly from its POD and leads to the decomposition A = $X'V\Sigma^{-1}U^{\dagger}$, with Σ^{-1} the inverse of Σ . To efficiently diagonalize the operator A, we compute the eigendecomposition of $\tilde{A} := U^{\dagger}AU$. \tilde{A} is the projection of A onto the span of U and is more convenient than A since the size is $r \times r$ (See step 2 of Fig. 3). The resulting eigen decomposition is $\tilde{A}W = \Lambda W$, with eigenvalues Λ as a diagonal matrix and eigenvectors W in $\mathbb{C}^{r\times r}$. To compute the dynamic modes Φ , we project W back into the x-dimension to obtain $\Phi = UW$. However, we do not explicitly compute the dynamic modes for predicting the dynamics. Instead, we predict the state of the system at a future time step k directly from the eigen decomposition of \hat{A} as:

$$\mathbf{u}_{T+k} := A^k \mathbf{u}_T = U \tilde{A}^k U^{\dagger} \mathbf{u}_T$$
$$= U W \Lambda^k W^{-1} U^{\dagger} \mathbf{u}_T.$$
(5)

where u_T is the spatial snapshot at time T. Since all matrix multiplications are achieved through local tensor contractions, the computational complexity of the MPS-DMD algorithm scales logarithmically with both N_x and N_t . This is in contrast with Ref. [33], which features a runtime scaling linearly with the number of snapshots N_t .

Now, we discuss the various methods for obtaining the MPS space-time encoding of the snapshot matrices. First, thanks to the MPS space-time solver, we can solve the governing PDE of the system and obtain the snapshot matrices directly from the MPS solution. However, we consider the general case with data that is not available in the MPS format. In this case, if the data is known to have an MPS structure, then the benefits of MPS-DMD far outweigh the overhead of finding the MPS representation. In practice, we observe that the bond dimensions are small, consistent with the decay of temporal entanglement shown in Fig. 2. Thus, we can obtain the MPS efficiently using methods such as optimized TT-SVD algorithms [46], TT-cross approximation [47], or streaming TT decompositions [48].

In particular, our method to compress an arbitrary data set is as follows. The snapshot matrix X'

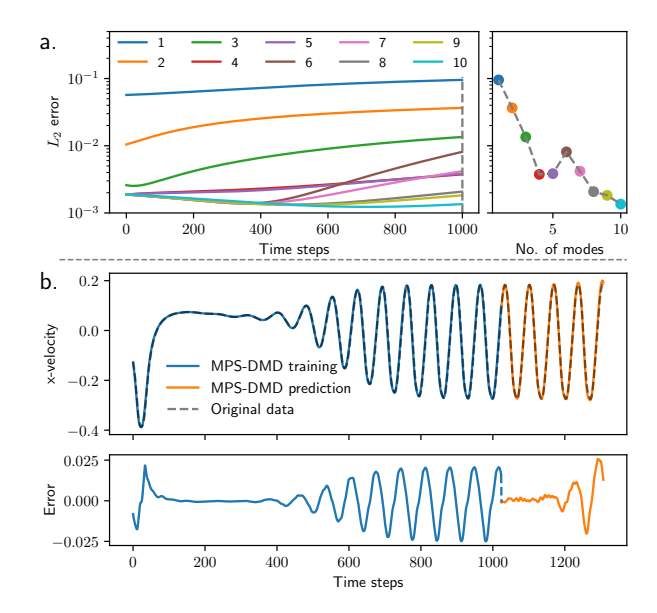


FIG. 4. MPS-DMD prediction of nonlinear systems. (a.) 1D Burgers' equation: We start with the MPS space-time solution of Burgers' equation for a fluid with viscosity $\nu = 10^{-3}$, on a $2^{10} \times 2^{10}$ grid in the (x,t) domain, obtained using the MPS space-time solver proposed in Sec. IIIB. We predict the solution for the next 1000 time steps using the MPS-DMD algorithm. We plot the behavior of the L_2 error of the predicted solution over time at different truncations of the spacetime bond dimension, which corresponds to the number of DMD modes used. (b.) 2D Kármán vortex street phenomena: Using simulated data from Ref. [49], we encode the time series of the x-velocity component into the MPS space-time representation. We choose the interleaved encoding (see Ref. [7]) for the 2D space, but maintain the space-time ordering of the MPS. We plot the x-velocity in the wake of the cylinder, which captures the vortex street phenomenon. Using only 100 DMD modes, we observe that the dominant characteristics of the velocity are recovered. We also note that even if the training error increases with time, the DMD modes generalize well for accurate predictions.

of size $N_x \times N_t$ is seen as:

$$X' = \sum_{i=1}^{N_t} \boldsymbol{u}_i \otimes \boldsymbol{e}_i \tag{6}$$

where e_i are the unit basis vectors for $i = 1, ..., N_t$. We compress each u_i snapshot of the data into MPSs of $\log_2(N_x)$ tensors, using TT-SVD. Next, we compute the space-time MPS by sequentially adding the snapshots stacked along with the corresponding MPS encoding of e_i , which has $\log_2(N_t)$ tensors and a bond dimension $\chi = 1$. By truncating the bond dimension after each addition, we efficiently find the space-time MPS with $\log_2(N_x) + \log_2(N_t)$ tensors.

In Fig. 4, we compute the MPS-DMD predictions

for two different nonlinear systems. In panel a., we start from the MPS space-time solution on a 1024×1024 grid for the (1+1)D Burgers' equation. We compare the prediction error of MPS-DMD for different truncations of the space-time bond dimension, which correspond to varying numbers of DMD modes used. We observe that the prediction error remains small for up to k = 1000 time steps into the future, despite the MPS representation having a bond dimension of only 10, resulting in a compression of over 99%. In panel b., we predict the 2D Karman vortex street phenomena using simulated data from Ref. [49]. Here, we use the above-described sequential addition method to compress the 2D velocity fields into their MPS representation. We observe that the MPS-DMD algorithm accurately predicts the dynamics of the Karman vortex street using only 100 DMD modes, capturing all the relevant information of the data in the MPS space-time representation with a memory reduction of 97.42%.

IV. CONCLUSIONS

We investigated the effectiveness of quantuminspired methods, based on the MPS encoding of the combined space-time domain, for both simulating and predicting dynamics. We developed two methods: MPS space-time solver and MPS-DMD, with the runtime scaling logarithmically in both spatial and temporal resolution. For both linear and nonlinear equations, we observed that the MPS spacetime solution captures all relevant spatio-temporal correlations with small bond dimensions, resulting in compression ratios exceeding 99%. Additionally, the MPS space-time ansatz appears to capture the separation of variables for PDEs. We leave the further analysis of this connection for future work. We observed that the long-term dynamics of both 1D and 2D nonlinear systems can be accurately predicted, with MPSs compressing more than 97% of the data. Here, we also note that the MPS ansatz imposes a hierarchical nature on the timescales of the dynamics. We believe that this could lead to improved DMD implementations, since it has been previously observed that DMD benefits from a separation between slow and fast dynamics [50].

This work also raises an important question regarding the role of quantum algorithms for solving PDEs. By treating the space-time domain simultaneously, the nature of temporal entanglement becomes a crucial metric in studying the separation between classical (quantum-inspired) and fully quantum approaches [51]. Finally, we remark that the MPS-DMD connection not only facilitates compressed data-driven approaches, with numerous potential applications, but also enhances the interpretability of MPSs. This highlights the role of tensor networks in bridging the gap between numerical methods and data-driven approaches.

V. ACKNOWLEDGMENTS

RP, SP, ET, and LA thank Jonas Fuska and Ingo Roth for engaging in fruitful discussions. NR and MKR gratefully acknowledge support from grant number KUEX-8434000491, a collaborative effort between Khalifa University, the Technology Innovation Institute, and the Emirates Nuclear Energy Company. This research was carried out by the Technology Innovation Institute and the Emirates Nuclear Technology Center, a collaboration among Khalifa University of Science and Technology, Emirates Nuclear Energy Company, and the Federal Authority for Nuclear Regulation.

C. Grossmann, H.-G. Roos, and M. Stynes, Numerical Treatment of Partial Differential Equations (Springer Berlin Heidelberg, 2007).

^[2] R. Orús, A practical introduction to tensor networks: matrix product states and projected entangled pair states, Annals of Physics 349, 117 (2014).

^[3] A. Cichocki, N. Lee, I. Oseledets, A.-H. Phan, Q. Zhao, and D. P. Mandic, Tensor networks for dimensionality reduction and large-scale optimization: Part 1 low-rank tensor decompositions, Foundations and Trends in Machine Learning 9, 249 (2016).

^[4] A. Cichocki, N. Lee, I. Oseledets, A.-H. Phan, Q. Zhao, M. Sugiyama, and D. P. Mandic, Tensor networks for dimensionality reduction and largescale optimization: Part 2 applications and future perspectives, Foundations and Trends in Machine

Learning 9, 431 (2017).

^[5] E. Kornev, S. Dolgov, M. Perelshtein, and A. Melnikov, Tetrafem: numerical solution of partial differential equations using tensor train finite element method, Mathematics 12, 3277 (2024).

^[6] R. D. Peddinti, S. Pisoni, A. Marini, P. Lott, H. Argentieri, E. Tiunov, and L. Aolita, Quantuminspired framework for computational fluid dynamics, Communications Physics 7, 135 (2024).

^[7] S. Pisoni, R. D. Peddinti, E. Tiunov, S. E. Guzman, and L. Aolita, Compression, simulation, and synthesis of turbulent flows with tensor trains, arXiv preprint arXiv:2506.05477 (2025).

^[8] N. Gourianov, M. Lubasch, S. Dolgov, Q. Y. van den Berg, H. Babaee, P. Givi, M. Kiffner, and D. Jaksch, A quantum-inspired approach to exploit turbulence

- structures, Nature Computational Science 2, 30 (2022).
- [9] M. Kiffner and D. Jaksch, Tensor network reduced order models for wall-bounded flows, Physical Review Fluids 8 (2023).
- [10] E. Ye and N. F. G. Loureiro, Quantum-inspired method for solving the Vlasov-Poisson equations, Phys. Rev. E 106 (2022).
- [11] N.-L. van Hülst, P. Siegl, P. Over, S. Bengoechea, T. Hashizume, M. G. Cecile, T. Rung, and D. Jaksch, Quantum-inspired tensor-network fractional-step method for incompressible flow in curvilinear coordinates, arXiv preprint arXiv:2507.05222 (2025).
- [12] D. P. Truong, M. I. Ortega, I. Boureima, G. Manzini, K. Ø. Rasmussen, and B. S. Alexandrov, Tensor networks for solving realistic timeindependent boltzmann neutron transport equation (2023), arXiv:2309.03347 [math.NA].
- [13] U. Schollwöck, The density-matrix renormalization group in the age of matrix product states, Annals of Physics **326**, 96 (2011).
- [14] F. Verstraete, V. Murg, and J. I. Cirac, Matrix product states, projected entangled pair states, and variational renormalization group methods for quantum spin systems, Advances in Physics 57, 143 (2008).
- [15] I. V. Oseledets, Tensor-train decomposition, SIAM Journal on Scientific Computing 33, 2295 (2011).
- [16] I. V. Oseledets and S. V. Dolgov, Solution of linear systems and matrix inversion in the TT-format, SIAM Journal on Scientific Computing 34, A2718 (2012).
- [17] V. A. Kazeev and B. N. Khoromskij, Low-rank explicit QTT representation of the laplace operator and its inverse, SIAM Journal on Matrix Analysis and Applications 33, 742 (2012).
- [18] L. Grasedyck, D. Kressner, and C. Tobler, A literature survey of low-rank tensor approximation techniques, GAMM-Mitteilungen 36, 53–78 (2013).
- [19] J. Latorre, Image compression and entanglement, abs/quant-ph/0510031 (2005).
- [20] M. Lindsey, Multiscale interpolative construction of quantized tensor trains, arXiv preprint arXiv:2311.12554 (2023).
- [21] N. Gourianov, Exploiting the structure of turbulence with tensor networks, Ph.D. thesis, University of Oxford (2022).
- [22] R. Courant, K. Friedrichs, and H. Lewy, Uber die partiellen differenzengleichungen der mathematischen physik, Mathematische Annalen 100 (1928).
- [23] T. Wick, Space-Time Methods (2023).
- [24] A. Schafelner, Space-time finite element methods (2021).
- [25] O. Steinbach and H. Yang, Space-time finite element methods for parabolic evolution equations: discretization, a posteriori error estimation, adaptivity and solution (2019).
- [26] S. V. Dolgov, B. N. Khoromskij, and I. V. Oseledets, Fast solution of parabolic problems in the tensor train/quantized tensor train format with initial application to the fokker-planck equation, SIAM Jour-

- nal on Scientific Computing 34 (2012).
- [27] T. Breiten, S. Dolgov, and M. Stoll, Solving differential Riccati equations: A nonlinear space-time method using tensor trains, Numerical Algebra, Control & Optimization 11, 407 (2021).
- [28] D. Adak, D. P. Truong, G. Manzini, K. Ø. Rasmussen, and B. S. Alexandrov, Tensor network space-time spectral collocation method for time-dependent convection-diffusion-reaction equations, Mathematics 12 (2024).
- [29] D. Adak, M. E. Danis, D. P. Truong, K. Ø. Rasmussen, and B. S. Alexandrov, Tensor network space-time spectral collocation method for solving the nonlinear convection diffusion equation, Journal of Scientific Computing 103 (2025).
- [30] L. Arenstein, M. Mikkelsen, and M. Kastoryano, Fast and flexible quantum-inspired differential equation solvers with data integration, arXiv preprint arXiv:2505.17046 (2025).
- [31] P. J. Schmid, Dynamic mode decomposition of numerical and experimental data, Journal of Fluid Mechanics 656, 5–28 (2010).
- [32] J. N. Kutz, S. L. Brunton, B. W. Brunton, and J. L. Proctor, *Dynamic Mode Decomposition: Data-Driven Modeling of Complex Systems* (Society for Industrial and Applied Mathematics, 2016).
- [33] S. Klus, P. Gelß, S. Peitz, and C. Schütte, Tensor-based dynamic mode decomposition, Nonlinearity 31, 3359 (2018).
- [34] G. H. Golub and J. M. Ortega, Chapter 5 Life Is Really Nonlinear, in Scientific Computing and Differential Equations: An Introduction to Numerical Methods (Academic Press, Boston, 1992) p. 167.
- [35] C. W. Rowley, I. Mezić, S. Bagheri, P. Schlatter, and D. S. Henningson, Spectral analysis of nonlinear flows, Journal of Fluid Mechanics 641, 115 (2009).
- [36] P. J. Schmid, Dynamic mode decomposition and its variants, Annual Review of Fluid Mechanics 54, 225–254 (2022).
- [37] I. A. Luchnikov, E. O. Kiktenko, M. A. Gavreev, H. Ouerdane, S. N. Filippov, and A. K. Fedorov, Probing non-markovian quantum dynamics with data-driven analysis: Beyond black-box machine-learning models, Physical Review Research 4 (2022).
- [38] M. J. Colbrook, The multiverse of dynamic mode decomposition algorithms, in *Handbook of Numeri*cal Analysis, Vol. 25 (Elsevier, 2024) pp. 127–230.
- [39] V. A. Kazeev, B. N. Khoromskij, and E. E. Tyrtyshnikov, Multilevel toeplitz matrices generated by tensor-structured vectors and convolution with logarithmic complexity, SIAM Journal on Scientific Computing 35, A1511–A1536 (2013).
- [40] D. V. Savostyanov and I. Oseledets, Fast adaptive interpolation of multi-dimensional arrays in tensor train format, The 2011 International Workshop on Multidimensional (nD) Systems, 1 (2011).
- [41] M. K. Ritter, Y. Núñez Fernández, M. Wallerberger, J. Von Delft, H. Shinaoka, and X. Waintal, Quantics tensor cross interpolation for high-resolution parsimonious representations of multivariate functions,

- Physical Review Letters **132**, 056501 (2024).
- [42] S. V. Dolgov and D. V. Savostyanov, Alternating minimal energy methods for linear systems in higher dimensions, SIAM Journal on Scientific Computing 36, A2248 (2014).
- [43] A. D. Polyanin and A. I. Zhurov, Separation of Variables and Exact Solutions to Nonlinear PDEs (Chapman and Hall/CRC, 2021).
- [44] G. Teschl, Ordinary differential equations and dynamical systems, Vol. 140 (American Mathematical Soc., 2012).
- [45] N. Rapaka et al., (in preparation).
- [46] M. Röhrig-Zöllner, J. Thies, and A. Basermann, Performance of the low-rank tt-svd for large dense tensors on modern multicore cpus, SIAM Journal on Scientific Computing 44, C287 (2022).
- [47] I. Oseledets and E. Tyrtyshnikov, TT-cross approximation for multidimensional arrays, Linear Algebra and its Applications 432, 70 (2010).
- [48] D. Kressner, B. Vandereycken, and R. Voorhaar, Streaming tensor train approximation, SIAM Journal on Scientific Computing 45, A2610 (2023).
- [49] J. Tencer, Cylinder in Crossflow (2020).
- [50] J. N. Kutz, X. Fu, and S. L. Brunton, Multiresolution dynamic mode decomposition, SIAM Journal on Applied Dynamical Systems 15, 713 (2016).
- [51] Y. Zhou, E. M. Stoudenmire, and X. Waintal, What limits the simulation of quantum computers?, Physical Review X 10, 041038 (2020).
- [52] W. L. Wood, An exact solution for burger's equation, Communications in Numerical Methods in Engineering 22, 797–798 (2006).
- [53] A. D. Polyanin and V. F. Zaitsev, Handbook of Nonlinear Partial Differential Equations (Chapman and Hall/CRC, 2016).
- [54] S. M. Filipov and I. Faragó, Implicit euler time discretization and fdm with newton method in nonlinear heat transfer modeling, arXiv preprint arXiv:1811.06337 (2018).
- [55] J. J. García-Ripoll, Quantum-inspired algorithms for multivariate analysis: from interpolation to partial differential equations, Quantum 5, 431 (2021).

Supplementary Information

Appendix A: Space-time MPS formulation

In this appendix, we present the construction of the *all-at-once* space-time linear system in Eq. (2), starting from the time-stepping equation. We also describe the corresponding MPS implementation.

First, we recall the standard (1+1)-dimensional time-dependent PDE of u from Eq. (1):

$$\partial_t^p u + F(u, \partial_x u, \dots, \partial_x^q u) = g(x, t)$$

For the sake of clarity, we stick to the first-order derivative in time, p = 1. We further set g(x,t) = 0. We start with the nonlinear case, i.e., where F is dependent on the solution u. Since the linear case is a simplified version, it follows straightforwardly.

After the discretization of the domain, we represent the discretized operator version of F with $\mathbb{F}(u)$ acting on the solution u. Then, for the implicit scheme, the time-stepping equation at time step j is given by:

$$\frac{u_{i,j+1} - u_{i,j}}{\tau} + \mathbb{F}(u_{i,j+1})u_{i,j+1} = 0. \tag{A1}$$

We define the implicit operator $\mathbb{O} = \mathbb{I} + \mathbb{F}(u)\tau$, such that Eq. (A1) is rewritten as $\mathbb{O}(u)\boldsymbol{u}_{j+1} = \boldsymbol{u}_j$, where \boldsymbol{u}_j is a column vector containing the solution at all spatial grid points and fixed time step j. We linearize the equation using Picard iterative update, where at iteration p the linear operator is given by substituting the solution at iteration p-1, i.e. $\mathbb{O}(\boldsymbol{u}_{j+1}^{p-1})\boldsymbol{u}_{j+1}^p = \boldsymbol{u}_j^p$. For the sake of brevity, we now refer to the linearized operator simply as \mathbb{O}_x .

We now look at the linear system for the entire space-time solution vector \boldsymbol{u} , given by the tensor product:

$$(\mathbb{O}_x \otimes \mathbb{I}_t) \boldsymbol{u} = \boldsymbol{u}^{\text{shifted}}, \tag{A2}$$

where \mathbb{I} is the identity operator and the subscripts x and t are used to emphasize the spatial and temporal operators. u^{shifted} denotes the space-time solution shifted backward by one time step τ . More explicitly, u and u^{shifted} are given by the element-wise stacking of vectors u_j :

$$\mathbf{u} = (u_{1,1}, u_{1,2}, ..., u_{1,N_t}, u_{2,1}, ..., u_{N_x,N_t})^T$$

$$\mathbf{v}^{\text{shifted}} = (u_{1,0}, u_{1,1}, ..., u_{1,N_t-1}, u_{2,0}, ..., u_{N_x,N_t-1})^T$$
(A3)

Additionally, $\boldsymbol{u}^{\text{shifted}} = (\mathbb{I}_x \otimes \mathbb{S}_t)\boldsymbol{u} + \boldsymbol{u}_0 \otimes \boldsymbol{e}_1$ where $\boldsymbol{e}_1 \in \mathbb{R}^{N_t}$ is the one-hot vector with value one in the first position and the shift operator \mathbb{S}_t is:

$$\mathbb{S}_{t} = \begin{pmatrix} 0 & 0 & 0 & 0 \\ 1 & 0 & 0 & 0 \\ 0 & 1 & 0 & 0 \\ 0 & 0 & 1 & 0 \\ & & \ddots & \ddots \end{pmatrix}_{N \times N} \tag{A4}$$

Finally, we build the *all-at-once* space-time linear system as:

$$(\mathbb{O}_x \otimes \mathbb{I}_t - \mathbb{I}_x \otimes \mathbb{S}_t) \boldsymbol{u} = \boldsymbol{u}_0 \otimes \boldsymbol{e}_1 . \tag{A5}$$

We remark that this is equivalent to Eq. (2). We now translate all the vectors and operators in Eq.(A5) into the MPS-MPO formalism.

The operator \mathbb{O}_x arises from spatial derivatives and functions of the solution in the case of nonlinear equations. The spatial derivatives require Toeplitz matrices, for which analytical MPO constructions are known [39]. All other matrices, such as identity or shift matrices, can also be seen as simple Toeplitz matrices with only one diagonal. The nonlinear functions of u can either be constructed from the powers of the MPS compressed with TT-SVD or using TT-cross interpolation directly from the MPS representing the solution [40, 41]. The tensorization in Eq.(A5) results in the concatenation of the constituent MPOs (and MPSs) for the spatial and temporal parts. This completes the assembly of the all-at-once linear system in the MPS format, which is then solved using DMRG-inspired algorithms. DMRG is a variational method that optimizes the MPS tensors locally, obtaining the MPS solution with a runtime scaling polynomially with the bond dimension χ , ranging from $\mathcal{O}(\chi^3)$ to $\mathcal{O}(\chi^6)$ depending on the variant [16, 42].

Appendix B: Numerical results

Here, we present the detailed numerical simulations using our MPS space-time solver. First, we focus on benchmarking against analytical solutions of paradigmatic PDEs. Next, we present more challenging regimes where no analytical solutions are known and compare the MPS solver against classical numerical methods.

1. Benchmarks

- a. Heat equation: The heat equation, or diffusion equation, $u_t \alpha \Delta u = 0$, is a paradigmatic second-order PDE that governs many interesting phenomena. It is a parabolic PDE, and is considered well-posed as an initial-boundary value problem. Here, we consider the equation over the domain $\Omega = (0, 2\pi) \times (0, T]$ with the initial condition $u_0(x) = \sin(x)$ and Dirichlet boundary conditions. The analytical solution for this equation is $u^*(x,t) = u_0(x)e^{-\alpha t}$. Using an MPS with 20 qubits, we encode the space-time solution for an evolution time of $T = 1024\tau$, where $\tau = 10^{-3}$.
- b. Wave equation: The 1D wave equation, $u_{tt}-ku_{xx}=0$, is a hyperbolic PDE which requires initial conditions on both u and u_t for being well-posed. We impose periodic boundary conditions in x and initialize the problem with $u(x,t=0)=\sin(\pi x)$ and $u_t(x,t=0)=0$. The analytical solution for this problem is given by $u^*(x,t)=\frac{1}{2}(\sin\left(\pi x+\sqrt{k}t\right)+\sin\left(\pi x-\sqrt{k}t\right))$. Using the MPS space-time solver, we find the discretized solution on a grid of $2^{10}\times 2^{10}$ points encoded in a 20-qubit MPS, for the domain $\Omega=(0,10)\times(0,T]$, where $T=1024\tau$ with $\tau=5\times 10^{-3}$.
- c. Burgers' Equation: In nonlinear problems, we first solve the 1D Burgers' equation, a fundamental equation that models the convection-diffusion process. It can be seen as a version of the 1D Navier-Stokes equations for a scalar variable. We use the MPS space-time solver for the linearized Burgers' equation and iterate until convergence. In Fig. A1c, we benchmark the solver for a specific instance where the analytical solution is known [52], given by $u^*(x,t) = \frac{2\nu\pi e^{-\nu\pi^2 t}\sin(\pi x)}{1.01+e^{-\nu\pi^2 t}\cos(\pi x)}$. By setting t=0, the necessary initial condition is obtained. We also find the appropriate homogeneous Dirichlet boundary conditions, i.e., u=0 at x=0 and x=1. We use a discretized domain of 2^{10} points in both x and t, and encode the solution in a 20-qubit MPS similar to the other cases. We plot the MPS solution after the iterative process has converged.
- d. Non-linear Schrödinger (NLS) equation: We now consider the NLS equation, which arises in quantum physics and has applications ranging from condensed matter systems to wave mechanics. Specifically, we consider the 1D 'focusing' case, defined by $i\psi_t = -\psi_{xx} 2|\psi|^2\psi$, where $\psi(x,t)$ is a complex-valued function for all $(x,t) \in [-3\pi,3\pi] \times (0,T]$. This equation admits an analytical solution, known as the bright soliton (see Appendix C for initial and boundary conditions), that we use to benchmark our space-time MPS solver. For all PDEs, we plot the MPS solutions and the absolute error with respect to the analytical solution in Fig. A1, along with the bipartite entanglement entropy of the solution. For nonlinear equations, we plot the solution and error at the final iteration. Additionally, we compute the entanglement entropy of the

intermediate Picard iterations.

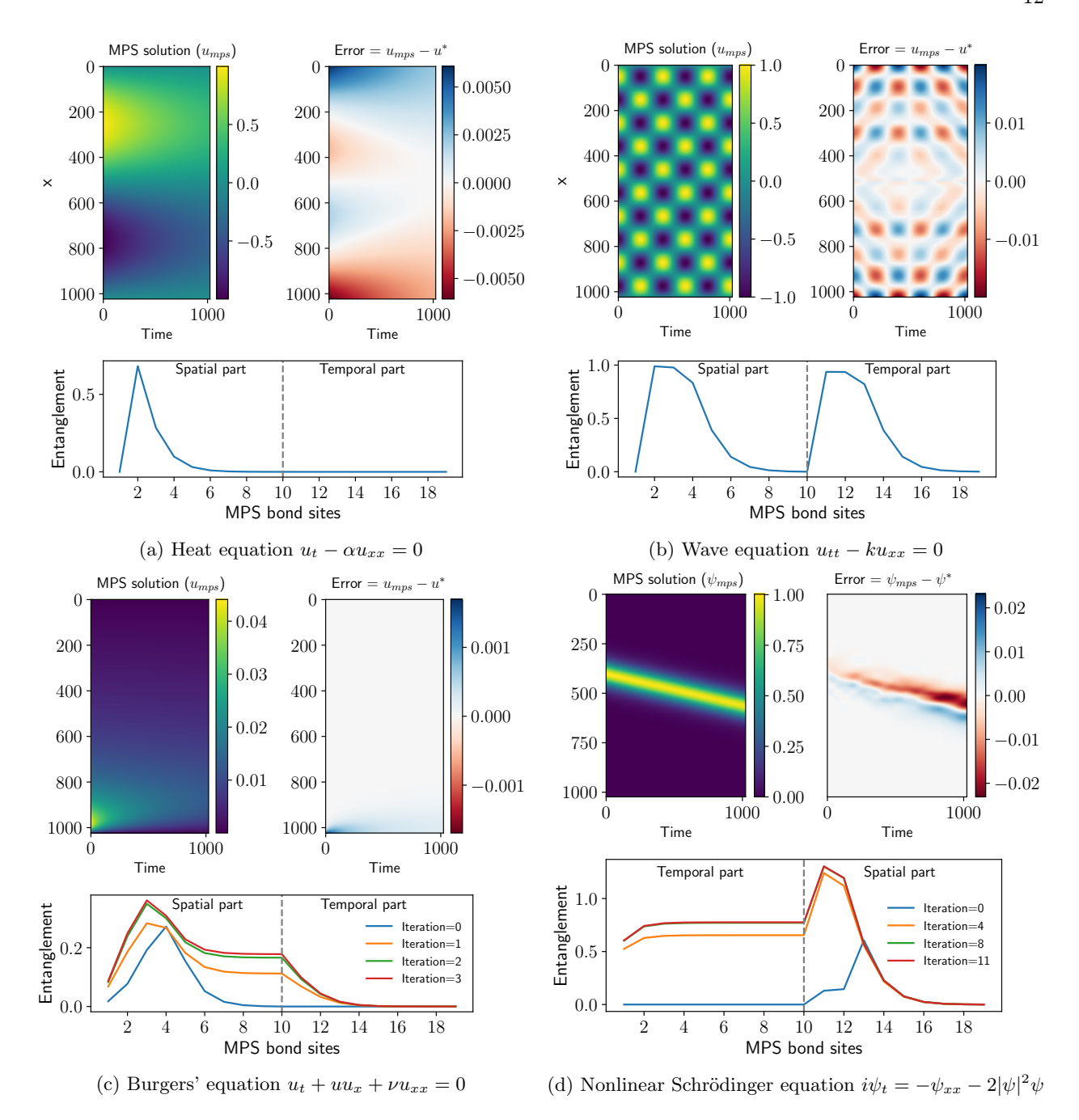


FIG. A1. Benchmarks of the MPS space-time solver. (a) We solve the 1D Heat equation $u_t - \alpha u_{xx} = 0$ with the initial condition $u(x,t=0) = \sin(x)$ on the domain $\Omega = (0,2\pi) \times (0,T]$. (b) We solve the 1D Wave equation $u_{tt} - ku_{xx} = 0$ with the initial conditions given by $u(x,t=0) = \sin(\pi x)$ and $u_t(x,t=0) = 0$ on the domain $\Omega = (0,10) \times (0,T]$. (c) We solve $u_t + uu_x + \nu u_{xx} = 0$ with the initial condition $u(x,t=0) = \frac{2\nu\pi\sin(\pi x)}{1.01+\cos(\pi x)}$. The solution is defined on the domain $\Omega = [0,1] \times (0,T]$. (d) We solve the 1D 'focusing' case of the NLS equation $i\psi_t = -\psi_{xx} - 2|\psi|^2\psi$, where $\psi(x,t)$ is a complex-valued function for all $(x,t) \in [-3\pi,3\pi] \times (0,T]$. We plot the magnitude of the solution in this case. For all equations, a 20-bit MPS encodes the solution, on the domain discretized by $2^{10} \times 2^{10}$ points on the x and x axes, respectively. The MPS space-time solution $u_{xx} = u_{xx} + u_{x$

2. Challenging regimes

Now, we present the cases for which no closed-form solutions exist. Additionally, the chosen regimes are such that the space-time methods are naturally suited, as the standard time-stepping scheme requires small time steps due to the nature of the discretized operators.

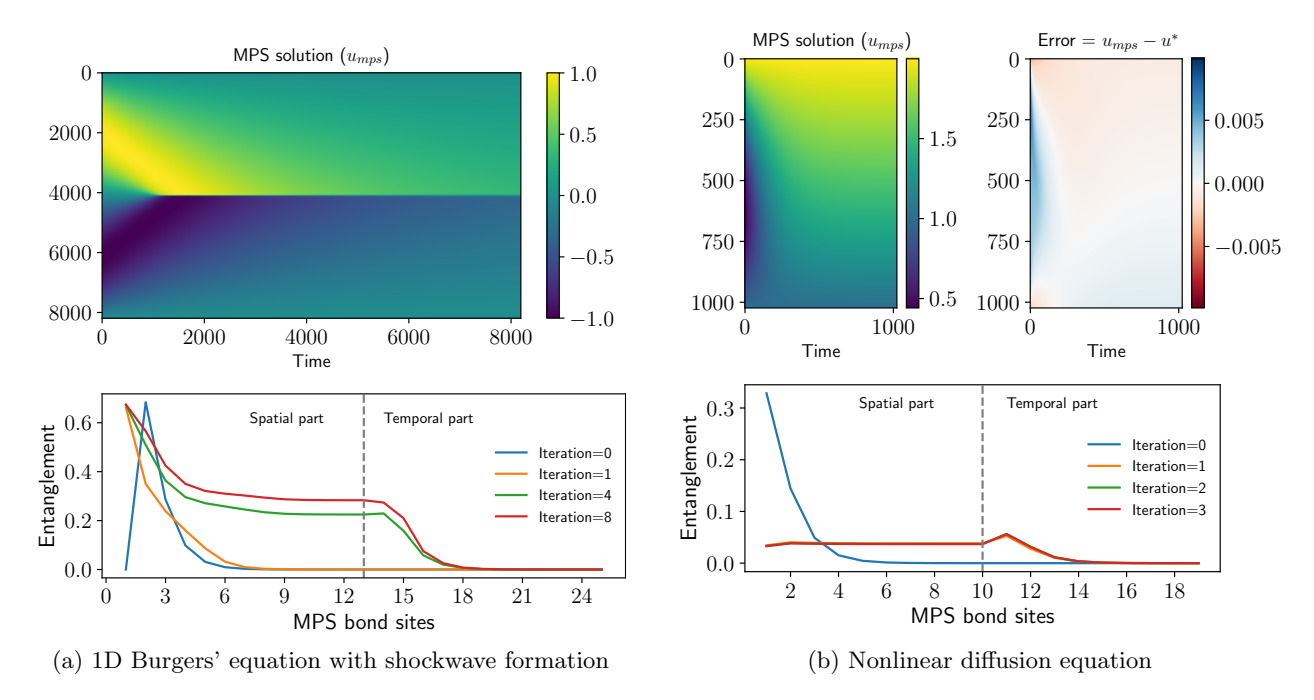


FIG. A2. MPS space-time solutions of the Burgers' and nonlinear diffusion equations.

a. Shockwave formation: In Fig. A2a, we solve for a more challenging regime of the 1D Burgers' equation, which leads to the formation of a shockwave. Here, we set the initial condition u(x,0) = sin(x) and the viscosity $\nu = 5 \times 10^{-3}$. We solve in the domain $[0, 2\pi] \times (0, N_t \tau]$ with 2^{13} points in both x and t, and $\tau = 10^{-3}$. We use a 26-qubit MPS with a bond dimension $\chi = 20$ for the MPS space-time solver. Here, the complete comparison of the MPS solution is not performed due to the lack of an efficient numerical solver at this grid size. Additionally, the analytical expansion based on Bessel functions is numerically unstable for evaluating the solution at small time steps.

b. Nonlinear Diffusion: We also solve the nonlinear diffusion equation, which is a nonlinear variant of the heat equation, modelling phenomena where the material properties depend on the temperature of the system. We consider the following setup:

$$\rho c_p \frac{\partial u}{\partial t} = \frac{\partial}{\partial x} \left(\kappa(u) \frac{\partial u}{\partial x} \right) , \qquad (B1)$$

where, $\kappa(u) = \kappa_0 \exp(\lambda u)$ and the initial condition is given by $u(x,0) = 2 - \frac{x-1}{2} + (x-1)(x-3)$, $x \in [1,3]$. We choose the specific initial condition for which analytical solutions are not available [53]. In Fig. A2b, we perform a similar benchmark as in Sec. B1 but against a standard numerical solver from Ref. [54]. Here, we choose $\kappa_0 = 0.1$ and $\lambda = 0.5$ and discretize the domain with 2^{10} points in both x and t dimensions. The resulting space-time solution is encoded in a 20-qubit MPS with a bond dimension $\chi = 10$.

Appendix C: NLSE time-space encoding

In this appendix, we motivate the time-space ordering of the MPS. Empirically, for the NLS equation, the MPS solver exhibits better convergence of the iterative linear system solver when the space and time legs

are swapped, i.e., switching from the space-time ordering to the time-space one. In the MPS representation, the time-space encoding is expressed by:

$$\psi = A_1^{(t_1)} A_2^{(t_2)} \dots A_m^{(t_m)} A_{m+1}^{(x_1)} A_{m+2}^{(x_2)} \dots A_{m+n}^{(x_n)}.$$
 (C1)

In this work, we consider the (1+1)-dimensional NLSE, described by:

$$i\frac{\partial\psi}{\partial t} = -\frac{\partial^2\psi}{\partial x^2} + \kappa|\psi|^2\psi , \qquad (C2)$$

where $\psi = \psi(x,t)$ is a complex-valued function for all $(x,t) \in [-3\pi, 3\pi] \times (0, T=3]$. We set $\kappa = -2$ (focusing case) and seek the bright soliton solution:

$$\psi(x,t) = q_0 \operatorname{sech}[q_0(x - x_0 - vt)] \exp\left[\frac{i}{2}v(x - x_0) + it(q_0^2 - \frac{1}{4}v^2)\right],$$
 (C3)

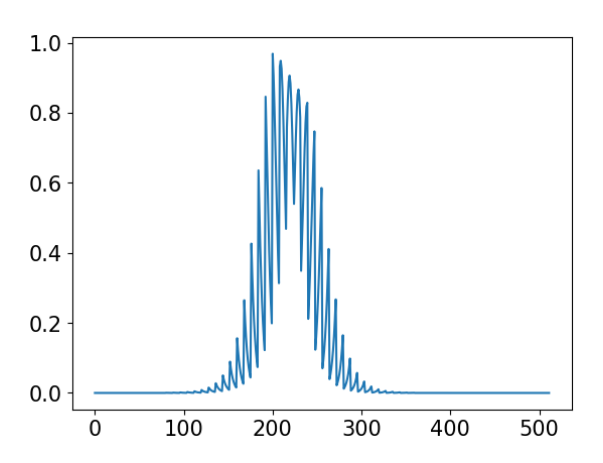
with q_0 representing the soliton amplitude, x_0 the initial soliton position, and v the propagation velocity. Following the procedure in Appendix A, the discretization of the time and space variables leads to:

$$\mathbb{O}_x = \mathbb{I}_x - i\tau(\partial_x^2 + 2|\psi|_x^2),\tag{C4}$$

such that $\mathbb{O}_x \psi_{j+1} = \psi_j$. This gives rise to the following all-at-once linear system:

$$(\mathbb{I}_t \otimes \mathbb{O}_x - \mathbb{S}_t \otimes \mathbb{I}_x) \psi = b . \tag{C5}$$

The results obtained using this encoding are reported in Sec. III and in Appendix B.



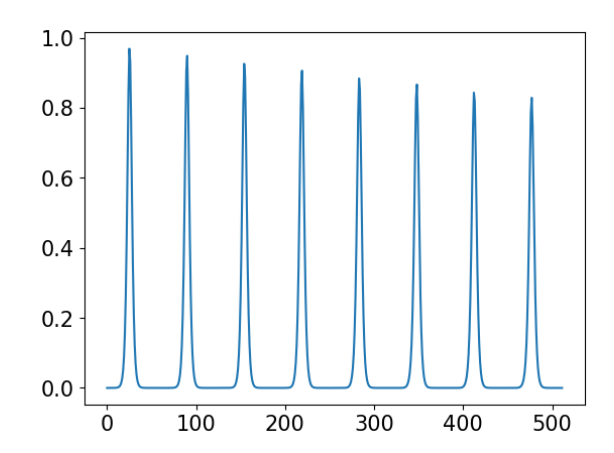


FIG. A3. Examples of the solution for different encodings. We report the magnitude of the MPS solution for the space-time (left) and the time-space (right) orderings on the reduced domain $(N_x = 6, N_y = 3)$ for a given iteration p. The space-time solution is oscillatory, with oscillations increasing both in amplitude and frequency as the total number of MPS tensors, i.e., the domain discretization, increases. In contrast, the time-space solution results in a smooth function regardless of the discretization, achieved by consecutively stacking simple functions at different times. The norm damping is an effect of the small values used for N_x and N_y .

We now comment on the motivation for using the time-space ordering. It is well established that smooth functions exhibit low-rank structure, i.e., compressibility [20, 55]. For this reason, one should aim at the ordering of the MPS tensors that corresponds to a well-behaved function. However, there are two limiting factors: first, establishing the optimal order is generally computationally expensive; second, we would like to keep the time and space legs separate, as this is a crucial step for the MPS-DMD algorithm presented in Sec. II C. Thus, we only test the time-space ordering and not the other mixed ones. In this scenario, the encoded solution at all times, $u_{t,x}$, is composed of stacking the spatial solutions at different times one after the other. This implies that the resulting solution will be smooth as long as the single-time solutions are smooth and the boundary conditions coincide at different times. On the other hand, the space-time ordering results in a highly oscillatory function. In Fig. A3, we report an example of such a solution for the propagating soliton. Our numerical findings confirm this intuition. We observe better convergence of the iterative solver and improved accuracy in the linear system solution (for a given iteration) when using the time-space ordering of the MPS tensors.